Atomistic modeling of defect-induced plasticity in CuNb nanocomposites

Enrique Martínez, Alfredo Caro, and Irene J. Beyerlein

Phys. Rev. B **90**, 054103 — Published 5 August 2014

DOI: 10.1103/PhysRevB.90.054103

Atomistic modeling of defect-induced plasticity in CuNb nanocomposites

Enrique Martínez,[1,*] Alfredo Caro,[1] and Irene J. Beyerlein[2]

[1] *Materials Science and Technology Division, MST-8, Los Alamos National Laboratory, Los Alamos, 87545 NM, USA*

[2] *Theoretical Division, T-3, Los Alamos National Laboratory, Los Alamos, 87545 NM, USA*

(Dated: July 21, 2014)

CuNb nanocomposites have proven stable under light-ion irradiation, although their response to heavy-ion bombardment and subsequent loading is still uncertain. In this paper we analyze the change in mechanical properties of model CuNb nanocomposites in vacancy supersaturated environments, mimicking certain effects introduced by heavy-ion irradiation. We have performed compression tests using molecular dynamics for different defect contents. The presence of defects substantially modifies the system response upon external loading. The dislocation nucleation mechanism changes with the interface atomic density. Stacking fault tetrahedra in the Cu layer may act as dislocation sources to lower significantly the yield stress and the same applies for voids present in the Nb layer. We have analyzed in detail the dislocation-interface interaction mechanisms under different conditions, showing how dislocations react with the misfit dislocations present at the interface to modify the atomic structure of the boundary, which suggests that the interface could be designed to optimize its defect healing properties. We conclude that heavy-ion irradiation softens the multilayer nanocomposites and that interfaces help in recovering these materials as they absorb the dislocations created from irradiation-induced defects.

PACS numbers:
Keywords: **Metallic Nanocomposites, Mechanical Response, Interfaces, Radiation Damage**

I. INTRODUCTION

In future fission and fusion nuclear reactors, extreme conditions of irradiation, temperature and corrosion, among others, are to be expected. These conditions call for the design of new materials able to sustain such conditions. In the specific case of irradiation, high neutron fluencies will have to be withstood by cladding and structural materials. This harsh environment leads to swelling, hardening, embrittlement, and in general, degrades material properties, driving the material to failure[1]. The reason for this failure is ultimately related to the creation of point defects and point defect clusters as the energetic neutrons collide with the atoms in the material, displacing them from their stable positions. If the material is designed such that the recombination and annihilation of defects is promoted, it is expected that such material could withstand higher doses of irradiation and therefore, are more suitable for the foreseen deleterious external conditions.

One way to mitigate irradiation damage is to introduce into the material structure stable sinks at which defects preferentially recombine and annihilate. It is well known that reduced dimensionality modifies the physical properties of the material. Heterophase nanolaminates with layer thicknesses in the order of nm's were shown to exhibit high flow strength and stable plastic flow to large strains[2]. It has also been observed that these materials are structurally stable under light ion bombardment since the high density of misfit dislocation intersections are preferential recombination sites and help self-anneal irradiation created defects[3–6]. A recent study by Zhang and Demkowicz[7], combining atomistic simulations with phase field modeling, shows that CuNb nanocomposites remain morphologically stable for layer thicknesses larger than 2-4 nm under neutron or heavy-ion irradiation. The role of interface boundaries in the mechanical response of irradiated materials have been studied mostly in the context of Hall-Petch relations[1] but few systematic studies are available in the literature focused on the relation between interface structure, irradiation damage and mechanical properties. One of these few examples is the estimation of hardening effects due to radiation damage in CuNb nanocomposites irradiated with He ions[5].

Neutron or heavy ion irradiation creates damage that might differ from light ion bombardment. In the latter, damage is produced homogeneously in the sample in the form of Frenkel pairs, while in the former damage manifests in the form of cascades, with defect clusters forming heterogeneously distributed in the material. This difference modifies the microstructure evolution and led to the development of the production bias model[8]. The production number of in-cascade created defects greatly depend on irradiation conditions, although the dependence on the material properties is much less pronounced[9]. Atomistic studies have shown that damage production becomes a linear function of the recoil energy after sub-cascade formation[10]. Commonly, vacancy and self-interstitial clusters are spatially segregated as vacancies agglomerate at the inner shell of the cascade while self-interstitials surround this inner region. Recent studies on defect formation and evolution in metals predict a distribution of cluster sizes mostly independent of the cascade energy[11–13]. Moreover, a power law for the self-interstitial cluster sizes in W[12] was shown to fit the atomistic data, with an unusual production of in-cascade large clusters. As described by the production bias model, the presence of

large clusters of defects generated in-cascade substantially modifies the microstructure evolution.

The modeling of the microstructure evolution of heterogeneous systems under irradiation is extremely complex. The main reason is that the irradiation process involves physics from very different time and length scales and cumbersome interaction mechanisms exist between defect clusters and among defect clusters and interfaces. Molecular dynamics (MD)[14] algorithms provide accurate insight into the ballistic mixing and thermal spike processes, but the thermal phase falls beyond its reachable time scale. Accelerated MD algorithms[15–17] extend the physical time that can be studied using MD approaches and provide good insight into complex mechanisms but their application is still limited in the system size as well as the simulated time. Adaptive kinetic Monte Carlo[18–21] is devised as one methodology that could, in principle, reach longer times, but still its computational efficiency is not good enough to model the thermal phase with full atomistic accuracy.

It is worth mentioning that materials in the proposed nuclear environments will be subjected to both radiation and mechanical deformation, although there is little understanding of the role of interfaces in these combined environments. In this work we focus on one portion of the problem, *i.e.*, how vacancies and vacancy clusters might modify the mechanical properties of a CuNb heterophase nanocomposite, and how interfaces respond upon deformation in the presence of irradiation created defects.

II. METHODOLOGY

Instead of running the whole dynamics of the process we have introduced in the microstructure different vacancy and vacancy cluster distributions. The cluster size distributions were chosen arbitrarily in order to highlight their effect on the mechanical properties of the material. Therefore, no relation between the defect distribution and recoil energies, or any irradiation condition, is established in this study. Once the defects have been added to the sample, compression tests at a strain rate of 10^7 s^{-1} and a temperature of 300 K have been performed to understand the basic mechanisms that take place in the deformation process and how defects influence the system response. Several calculations have been carried out at lower temperature (10 K) also, in which we observed that the main deformation processes remain unchanged as thermally activated events are suppressed. The simulations below have been performed with the MD code LAMMPS[22], using an embedded atom method potential[23]. The system is periodic in the three directions and contains two heterophase interfaces with a Kurdjumov-Sachs (KS) orientation relationship such that the interface plane is $\{111\}$fcc $||$ $\{110\}$bcc and within the interface plane, $\langle 110\rangle$fcc $||$ $\langle 111\rangle$bcc. Each layer has a thickness of 7.5 nm. The reference base in the Cu layer is given by $x = [11\bar{2}]$, $y = [\bar{1}10]$ and $z = [111]$.

III. RESULTS

A. Dependence of dislocation nucleation stress with interfacial atomic density

In the pristine sample case, Shockley partial dislocations nucleate along the misfit dislocation cores at the interface and they glide into the Cu layer. The interface structure and the dislocation nucleation mechanisms for different types of interfaces in the CuNb system have been analyzed in detail in Refs. 24,25.

For the first set of calculations, vacancies were introduced at one interface according to a potential energy criterion: atoms with a potential energy larger than -3.30 eV (case 1), -3.40 eV (case 2), -3.45 eV (case 3) and -3.50 eV (case 4) were removed from the simulation box. These were Cu atoms at the misfit dislocation intersection (MDI) or misfit dislocation cores. The first value gives around one vacancy per MDI, the second about 3 vacancies per MDI, the third between 5 and 6 vacancies and the last one gives between 22 and 23 vacancies at the MDIs and dislocation cores. These values correspond to an atomic density in two atomic layers at the interface of 0.99, 1.01, 0.93 and 0.65 respectively, measured in the relaxed structures. Note that in case 2 the density of the interface is larger than in the pristine case as atoms relaxed to lower the created strain.

In cases 1, 2 and 3, Shockley partial dislocations nucleate at the interface on the Cu side as in the pristine case. Likewise, nucleation takes place along the misfit dislocations on a $\{111\}$ plane. A trailing partial is nucleated thereafter such that the whole dislocation with Burgers vector $\mathbf{b} = \frac{a_0}{2}[01\bar{1}]$ glides away from the interface. According to the dislocation extraction algorithm (DXA)[26], in all these three cases, the leading and trailing partials have Burgers vectors equal to $\mathbf{b}_{p1} = \frac{a_0}{6}[\bar{1}1\bar{2}]$ and $\mathbf{b}_{p1} = \frac{a_0}{6}[12\bar{1}]$, respectively, both gliding on a $\{1\bar{1}1\}$ plane. The nucleation stress is analogous to that of the pristine sample as is the deformation mechanism since the vacancy defects at the interface have not sufficiently altered the interface structure. On the other hand, for case 4, the stress required to nucleate the first defect is much lower than in the previous cases (Von Mises stress versus strain for the pristine sample and cases 1, 2, 3 and 4 is plotted in Fig. 1). In this latter case, instead of an intrinsic stacking fault, a high energy $\{111\}$ extrinsic fault is nucleated at the interface. The Shockley partial at the front of the extrinsic stacking fault is characterized by the Burgers vector $D\beta$. These results imply that the presence of a larger number of defects at the interface modifies the deformation mechanism, which lowers the stress required to nucleate the plasticity carrier, in this case, favoring extrinsic versus intrinsic stacking fault nucleation. Figure 2 shows the nucleation events for the four cases previously mentioned. A possible explanation for the transition in nucleation behavior will be presented in Sec. IV A.

As it was mentioned in the Introduction, neutron irra-

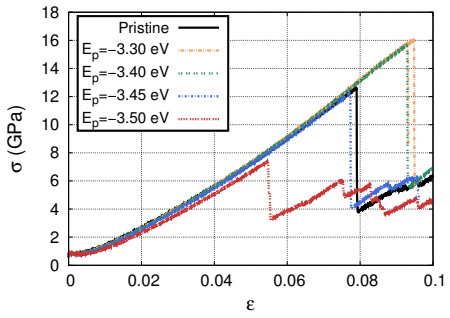

FIG. 1: (Color online) Von Mises stress versus strain for different vacancy contents at the KS interface.

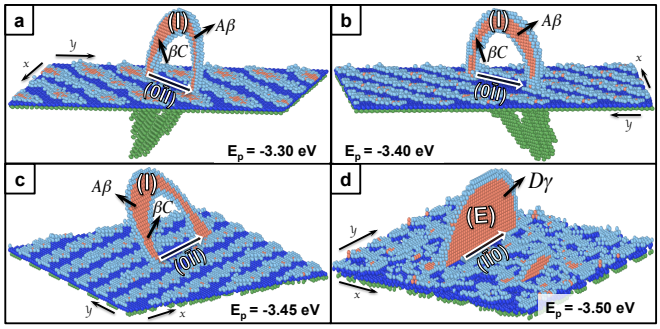

FIG. 2: (Color online) Dislocation nucleation in a CuNb nanocomposite under compressive strain. (a) Atoms with a potential energy greater or equal to -3.30 eV are removed; (b) Atoms with a potential energy greater or equal to -3.40 eV are removed; (c) Atoms with a potential energy greater or equal to -3.45 eV are removed; and (d) Atoms with a potential energy greater or equal to -3.50 eV are removed. According to a common neighbor analysis (CNA)[27], orange atoms are hcp, atoms in nonlinearly perturbed positions are shown in blue (Cu) and green (Nb).

diation generates segregated defects inside the displacement cascades. Voids, in the case of bcc materials, and SFTs, for fcc crystals, are typical examples of defects created in-cascade. These defects might act as dislocation sources upon application of stress[28,29]. In the following three sections, we study the competitive nature of defects as dislocation sources compared to the pristine interface sample and analyze in detail the dislocation nucleation events as well as the dislocation-interface interactions. We first consider only SFTs in the fcc layer, then only voids in the bcc layer in the following section, and finally both defects in the last section.

B. Effect of SFT on the dislocation nucleation mechanism

Stacking fault tetrahedra are ubiquitous defects in fcc materials. They form as a result of the collapse of voids since they are energetically favorable[30,31]. It has been shown that they can be produced directly in displacement cascades[32] in Cu. SFTs are characterized by a set of stair-rod dislocations limiting two intrinsic stacking faults. To study their effect in the mechanical properties of heterophase nanocomposites we have introduced two SFT distributions, differing in size and space. The first configuration contains two (perfect) SFTs, one collapsing from 66 vacancies and a second one from 105. The second configuration was created with five SFTs, of sizes 66, 105, 78, 91 and 120 vacancies respectively. The defect density was chosen to exacerbate the effect of the SFTs on the material response. Figure 3 shows these two initial configurations. Because of the limited layer thickness some of the in-cascade created SFTs could naturally intersect the interface, and therefore, we have generated the defects allowing for this possibility.

To explore their response under mechanical stress, we have subsequently applied normal strain in the z direction, perpendicular to the interface. Figure 4 shows the Von Mises stress versus strain for the pristine sample and those with SFTs. We observe that the stress at the yield point significantly reduces in the presence of the SFT defects with respect to the pristine sample. For the configuration with two SFTs the yield point stress reached 6.9 GPa, while for the sample with five SFTs the stress was about 6 GPa. The reason for this drastic drop in the yield point is that dislocations are emitted from the SFTs, instead of from the CuNb interface.

We find that a dislocation can be produced by a mechanically induced SFT unfaulting process. Figure 5 shows the unfaulting process by which the larger SFT (in the two SFT configuration) becomes a dislocation source. The process is identical for the configuration with five SFTs. In both cases the largest SFT in the system was the one that unfaulted and provided the gliding dislocations to accommodate the applied strain. Figure 6 sketches the process showing the stacking fault area and the Burgers vectors in Thompson notation. Figure 6[a] shows the unfaulting of the SFT, which follows the inverse process of SFT formation from a Frank loop. The following step (Fig. 6[b]) creates the Frank loop as the Shockley partials react with the stair-rod dislocations. Frank partials dissociate into a Shockley partial and a stair-rod. The extrinsic stacking fault is shown in light brown while the intrinsic stacking fault is plotted in green. The extrinsic fault is energetically unfavorable which assists in the nucleation of the trailing partial. Therefore, the stair-rod at the edge of the SFT base dissociates into two Shockley partials that sweep both the extrinsic and intrinsic stacking faults that were bounded by the stair-rod (Fig. 6[c]). Finally, after a series of dislocation reactions depicted in the figure a perfect segment with Burgers vector CD is formed in one end, bounded by two dissociated segments with an extrinsic fault between the partials. This perfect segment glides undissociated on a {100} plane until it reaches the interface where it is reflected and dissociates on a {111} plane in the Cu

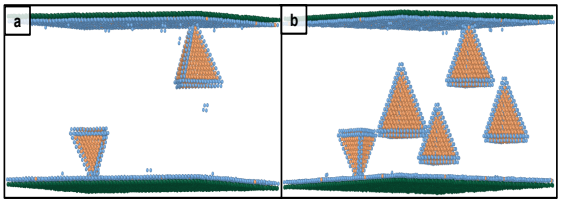

FIG. 3: (Color online) Initial configuration of samples with (a) two SFTs and (b) five SFTs in the Cu side of the nanocomposite. According to a common neighbor analysis (CNA)[27], orange atoms are hcp, Cu atoms in nonlinearly perturbed positions are shown in blue and Nb atoms in nonlinearly perturbed positions are displayed in green.

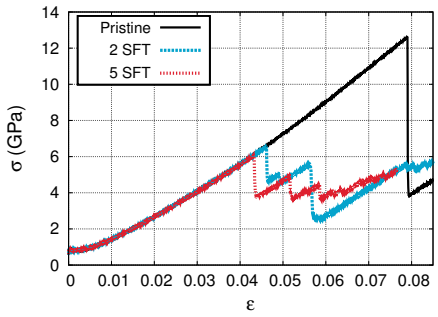

FIG. 4: (Color online) Von Mises stress versus strain for the systems containing two and five SFTs compared to the pristine sample.

layer. We will return to this interesting interaction in the discussion section (Sec. IV B).

This SFT unfaulting process is different than those reported previously. Recently, we have analyzed the behavior of Au nanopillars in the presence of SFTs[28], showing the process for the SFT to become a dislocation source. In this latter case, the pillar was {001}-oriented, which results in a different unfaulting process than the one observed here and makes possible that the SFT remains as an inexhaustible dislocation source. In the current nanocomposite configuration, the SFT disappears, turning into two threading dislocations, and therefore, no dislocation source remains in the system.

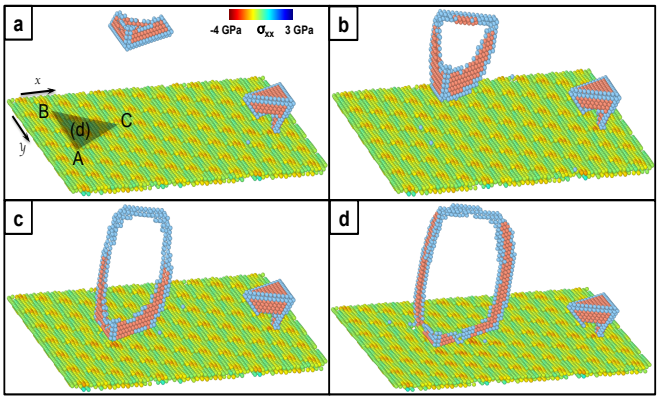

FIG. 5: (Color online) SFT unfaulting process in the sample with two SFTs. Two threading dislocations generate from one of the SFTs, accommodating the plastic deformation. According to a common neighbor analysis (CNA)[27], orange atoms are hcp, atoms in nonlinearly perturbed positions are shown in blue (Cu). Atoms at the interface are colored according to their σ_{xx} stress component.

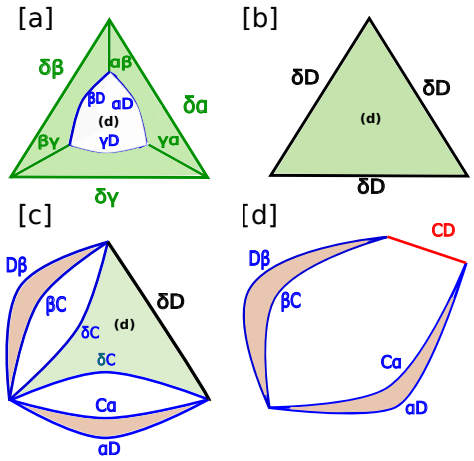

FIG. 6: (Color online) Analysis of the SFT unfaulting process. Burgers vectors are represented in Thompson notation. Green, blue and red lines represent stair-rod, Shockley partials and perfect dislocation respectively. Green areas are intrinsic stacking faults while brown areas represent extrinsic stacking faults.

C. Effect of voids on the dislocation nucleation mechanism

Voids are also formed directly in displacement cascades. In bcc systems, the stacking fault energy is usually higher than in fcc, which stabilizes the voids with respect to the SFTs. We have followed the same methodology as above and we have introduced two different void distributions in the Nb layer of the sample, intensifying the defect density to better study their effect on the system response. The first configuration contains two voids of 1.0 and 1.2 nm radius, while the second configuration involves four voids of radius 1.0, 1.2, 1.5 and 2.0 nm (see Fig. 7), randomly placed in the sample (note that they might interact with the interface). Figure 8 shows the stress-strain response of such systems under compressive external conditions. Again, as it was the case for the SFTs, the yield stress drastically decreases in the presence of voids. Dislocation loops with pronounced edge character are primarily nucleated at the voids at a level of stress lower than the one required for the dislocations to nucleate at the interface. Voids shrink as these

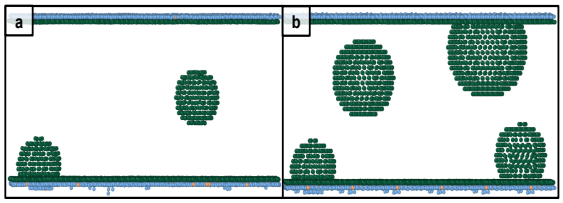

FIG. 7: (Color online) Initial configuration of samples with (a) two voids and (b) four voids in the Nb layer of the nanocomposite. Color coding same as in Fig. 3.

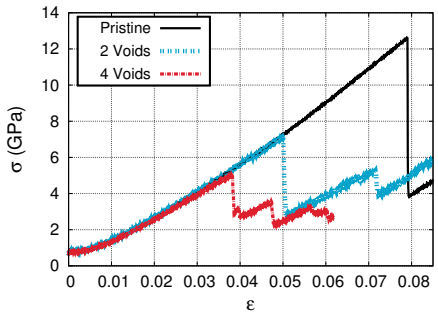

FIG. 8: (Color online) Von Mises stress versus strain for the systems containing two and four voids compared to the pristine sample.

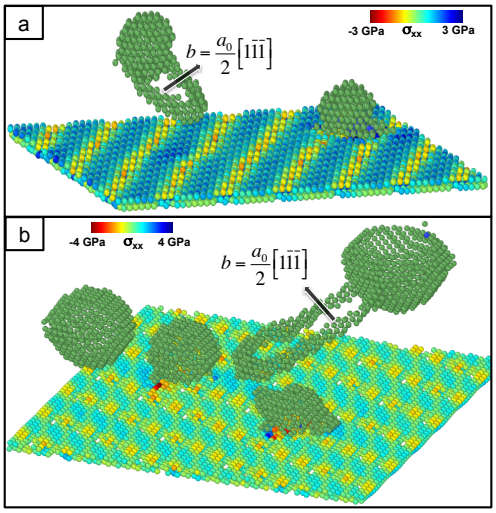

FIG. 9: (Color online) Dislocation nucleation process: (a) and (b) in the system with two voids; and (c) and (d) in the system with four voids. A shear dislocation loops is nucleated from a void in the Nb side and a perfect dislocation nucleates in the Cu layer. According to CNA[27] atoms in nonlinearly perturbed positions are shown in green (Nb). Atoms at the interface are colored according to their σ_{xx} stress component.

loops transport vacant volume to the interface, gliding on {110} planes towards the interface where they are finally absorbed. The nucleation of these loops slightly reduces the stress, although the yield point is characterized by the nucleation of dislocations from the interface into the Cu layer.

To understand the effect of the interaction between a void and the interface in the dislocation nucleation process, we have repeated the calculations in a sample with two voids in which neither of them intersects the interface. In this last case the yield stress is insignificantly higher than when the void and the interface initially interact, and therefore, the intersection seems not to help in the nucleation of dislocations on the Cu side.

D. Effect of SFTs and voids on the dislocation nucleation mechanism

Generally, defects are likely to be generated in both layers of the bimetal nanocomposite. To investigate the possible interactions between them, the last calculation we have carried out combines the presence of SFTs and voids in the mechanical response of the system. Figure 10 shows the initial configuration, with a distribution of five SFTs in the Cu layer (same distribution as in the five SFTs case above) and four-void in the Nb side (same distribution as in the four voids case above). The stress-strain response of the system to a external compressive strain is shown in Fig. 11. We see that the yield point in this last case is marginally lower than in the previous results. One of the SFTs acts as a dislocation source, following the same mechanism as shown in Figs. 5 and 6. The SFT that unfaults is the one closest to the intersection of the largest void with the interface, which was not the same in the case with five SFTs (shown with an asterisk in Fig. 10). The stress field of the void into the Cu side aids to the SFT unfaulting and slightly lowers the stress required to nucleate the partial dislocations from the SFT. It is worth noting that according to Figs 4 and 8, the yield stress in the presence of voids seems to be lower than the SFT unfaulting. It is precisely the interaction between defects that lowers the nucleation stress that leads to the unfaulting of the SFT prior to the loop nucleation.

Clearly, the configuration resulting from actual heavy-ion irradiations will not correspond to the constrained structures studied in this work. The density of defects will most certainly be lower and the interaction of vacancies with self-interstitials will modify the interface atomic structure. Self-interstitials diffuse faster than vacancies, and therefore, since interfaces represent strong sink for these defects, they will reach the interface and will be trapped by it, leading to a vacancy supersaturated environment within the layers. In this scenario, mechanisms like self-interstitial reemission[33] might be important in annihilating defects and self-annealing the material.

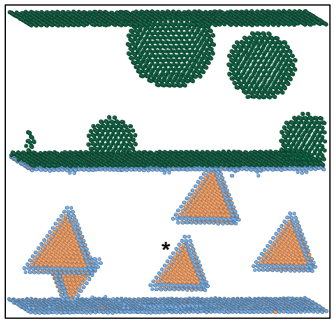

FIG. 10: (Color online) Initial configuration of a sample with five SFTs in the Cu layer and four voids in the Nb side of the nanocomposite. Color coding as in Fig. 3.

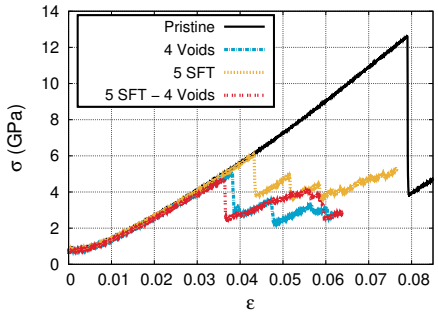

FIG. 11: (Color online) Von Mises stress versus strain for the systems containing four voids in the Nb layer and five SFTs in the Cu side compared to the pristine sample.

IV. DISCUSSION

A. Dependence of dislocation nucleation stress on interfacial atomic density

Figure 12 shows the relaxed atomic structure at 0 K of the KS interface depending on its density. We observe that the presence of vacancies modifies considerably the interface structure. As the atomic density decreases the structure becomes less well defined and the interface thickens. The misfit dislocations largely delocalize, which leads to the difference in the nucleation mechanism previously observed, starting from intrinsic stacking faults at large atomic densities to extrinsic faults at lower densities. Note (Fig. 2) that when an intrinsic fault forms, the Shockley partial has a tangent lying on the $\mathbf{t} = [0\bar{1}1]$ direction, close to the set of misfit dislocations with Burgers vector $\mathbf{b}_I^{(2)} = (0.00, 2.70, 0.00)$ (Å) of the pristine sample (see Fig. 14), in agreement with Zhang *et al.*[24]. The Shockley partial that was observed to nucleate first was the $\mathbf{A}\beta$. The $\mathbf{A}\beta$ segment reduces the strain energy compared to the $\beta\mathbf{C}$ partial since its dot product with $\mathbf{b}_I^{(2)}$ is lower, and therefore, the interface energy change after nucleation is less than it would be if they were not aligned. Zhang *et al.*[24] observed the opposite behavior as the nucleated dislocation had a Burgers vector $\beta\mathbf{C}$, which they explained in terms of self-energy of the dislocation at the interface. The authors showed that the self-energy of the $\beta\mathbf{C}$ partial is lower than that of the $\mathbf{A}\beta$. Their calculations were performed at 0 K, and therefore, one possible explanation for this discrepancy is that the nucleation rate at 300 K depends on entropic contributions that favor $\mathbf{A}\beta$ versus $\beta\mathbf{C}$, although the lower interface energy reasoning seems like a more plausible explanation.

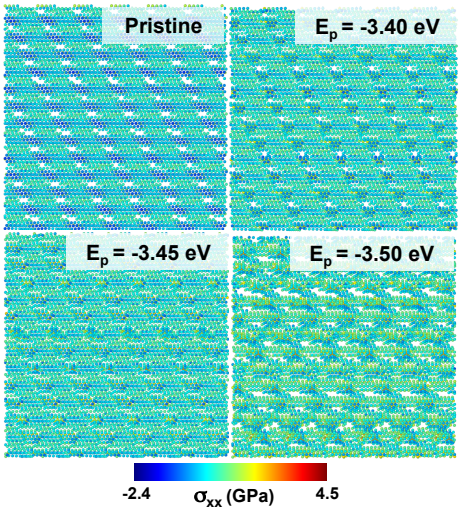

FIG. 12: (Color online) Von Mises stress versus strain for the systems containing four voids in the Nb layer and five SFTs in the Cu side compared to the pristine sample.

As the misfit dislocation arrangement changes with the presence of defects, the nucleation properties are modified and as a result an extrinsic fault is emitted as shown in case 4. The Shockley partial at the front of the extrinsic fault lies on a $\mathbf{t} = [1\bar{1}0]$ direction. The Burgers vector of the partial was $\mathbf{D}\gamma$. According to Zhang *et al.*[24] the Schmid factor for this dislocation points toward the interface and therefore it would be hindered. However, the discreteness of the interfacial dislocations is lost when a critical interfacial atomic density is reached and hence what nucleates follows a different set of rules. The nucleation of the extrinsic fault must be driven by local stress concentrations that develop when the highly defective interface is strained. Figure 13 shows the atomic structure of the extrinsic fault with an analysis of the dislocations Burgers vector (Fig. 13[a]) and the stacking sequence (Fig. 13[b]).

B. Dislocation-interface interaction in the Cu layer

In Sec. III B we have studied how the dislocation segments generated from the SFT interact with the interface. The KS interface in CuNb nanocomposites is characterized by two sets of misfit dislocations[25]. The

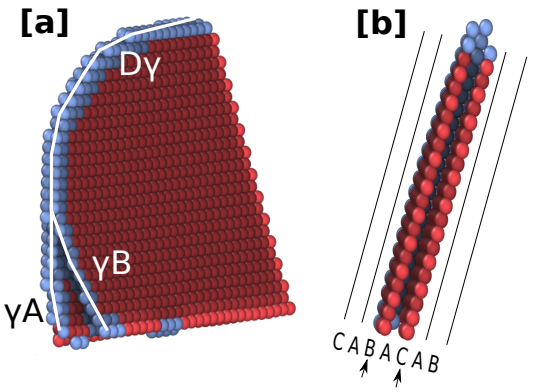

FIG. 13: (Color online) Burgers vector analysis and stacking sequence of the extrinsic fault generated under {111} compression for case 4.

Burgers vector of these dislocations have been calculated to be $\mathbf{b}_I^{(1)} = (-2.54, -1.56, 0.00)$ (Å) and $\mathbf{b}_I^{(2)} = (0.00, 2.70, 0.00)$ (Å) in the sample framework[25](see Fig. 14). The $\mathbf{b}_I^{(1)}$ set lays exactly in the $[1\bar{1}0]$ direction while the $\mathbf{b}_I^{(2)}$ set deviates about 5^o from the $[0\bar{1}1]$. The glide planes of the dissociated dislocations emitted from the SFT intersect the interface in the $[1\bar{1}0]$ and $[0\bar{1}1]$ directions. As the leading partials interact with the interface they react in the following way:

$$\begin{aligned} \mathbf{b}_I^{(1)} + \alpha D &= (-2.30, -1.14, 1.39) \\ \mathbf{b}_I^{(2)} + D\beta &= (0.24, 2.28, 1.39) \end{aligned} \qquad (1)$$

In both cases the total amount of strain reduces after the dislocation reactions. This favors their absorption. In contrast, the reaction of the trailing partials ($C\alpha$ and βC) with the new interface configuration is not energetically favorable and we have not seen their absorption at the interface in our simulations. On the other hand, we observe complete absorption of the full dislocations (CD) at the MDIs where the amount of strain is large and linear elasticity does not hold any longer. Figure 14 shows the resulting atomic microstructure with the remaining partial dislocations between MDIs.

The remaining perfect segment (CD) from the SFT unfaulting is mostly edge in character and glides on a 100 plane, which corresponds to nonorthorhombic slip in fcc materials. The dislocation tangent does not align with any misfit dislocation at the interface. In spite of that, the dislocation is absorbed upon interaction with the interface inducing a rotation on the misfit dislocation segments according to its Burgers vector. The strain energy accumulated at the interface is large enough to emit a new dislocation. Figure 15 shows the process of absorption of the perfect dislocation (Fig. 15[a]) gliding on a {100} plane and the reemission of a fresh dislocation (Fig. 15[b]) gliding on a {111}. Unlike the process above, this is not full absorption. This sequence of absorption

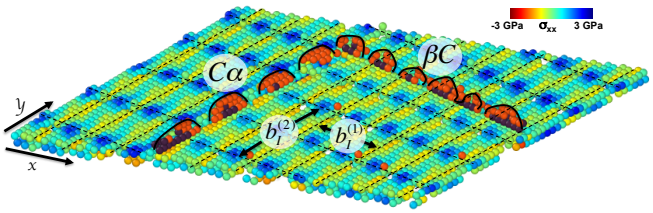

FIG. 14: (Color online) Interaction of partial dislocations generated at an SFT with a KS interface in CuNb. Neither bcc nor fcc atoms are shown. The gliding partials and the stacking fault are shown in red and dark purple, respectively. The interface is colored according to the σ_{xx} component of the atomic stress tensor. Solid and dashed lines mark the misfit dislocations, characterized by Burgers vectors $\mathbf{b}_I^{(1)}$ and $\mathbf{b}_I^{(2)}$. The Burgers vectors of the remaining partial dislocations at the interface are shown in Thompson notation.

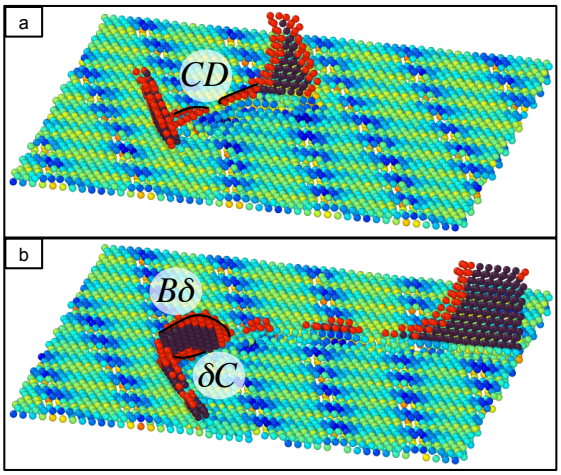

FIG. 15: (Color online) Interaction of a perfect dislocation generated at an SFT with a KS interface in CuNb. a) Absorption of the perfect segment at the interface; and b) Emission of a new dislocation in the Cu layer. Shown atoms and color coding as in Fig. 14.

and re-emission into the same crystal is together termed 'reflection'. The latter action lowers the energy of the interface and does work as plasticity can be carried on a stress-driven slip system.

We have also checked the effect of stress direction in the interaction of dislocations with the interface. We have applied strain in the direction [110] parallel to the interface plane. Again, a dislocation is nucleated from the SFT, although the mechanism is different compared to the one shown above. The stair-rod $\gamma\beta$ decomposes into γA and $A\beta$ and the stair-rod $\beta\alpha$ into βC and $C\alpha$. The two Shockley partials $A\beta$ and βC glide on the (b) plane to remove the stacking fault making up the SFT faces. The created dislocation, with full Burgers vector

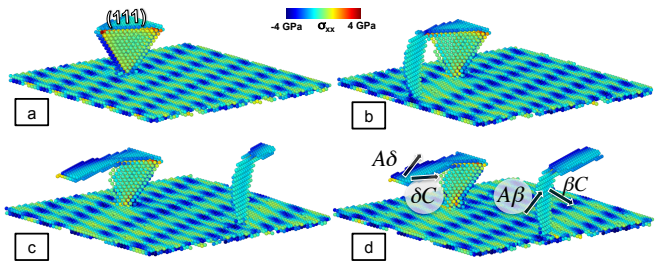

FIG. 16: (Color online) Process of nucleation of a dissociated dislocation from the SFT and its reaction with the misfit dislocations. Atoms colored according to the σ_{xx} component of the atomic stress tensor.

AC, reacts with the $\mathbf{b}_I^{(2)}$ as

$$\mathbf{b}_I^{(2)} + AC = (-2.20, 1.43, 0) \qquad (2)$$

that again lowers the total strain energy. Figure 16 shows the process. We observe how as the AC dislocation glides reacting with the $\mathbf{b}_I^{(2)}$ misfit dislocations, the structure of the interface changes, with the interface dislocations relocating to accommodate the new stress state. It is worth noting that the dislocation glides on two different {111} planes with a constriction forming at the point where planes change. The level of stress for the SFT to unfault is on the same order as the value obtained when the stress applied is perpendicular to the interface.

C. Prismatic loop-interface interaction in the Nb layer

To better understand the prismatic loop nucleation and the subsequent loop-interface interaction, one void was created in the Nb layer and compression strain was applied perpendicular to the interface at 10 K, in a similar way as in previous calculations. Prismatic loops are emitted from the void with an edge character as shown in Fig. 17[a], which represents a snapshot of the simulation analyzed with DXA[26]. The loop glides in {110} planes until it interacts with the interface. Upon contact, the dislocation loop leaves a depression in the Cu side surrounded by delocalized atoms in the form of a crater. Figure 17[b] shows the atomic structure (neither bcc nor fcc) of the interface after the absorption of the loop, with atoms colored according to their coordinate perpendicular to the interface. The vacancy formation energy in Cu is much lower than in Nb[24]. This thermodynamic driving force combined with the mixing energy of Cu into Nb makes the vacancy content of the loop move to the Cu side pushing some Cu atoms into the Nb layer. After the absorption of the loop the simulation run for 4.5 ns but no dissolution of the vacancy platelet, or formation of SFTs was observed. These craters act as stress concentrators and will increase the probability for dislocation nucleation, which eventually occurs in the simulation. This result is an indication that vacancy aggregates are at least metastable at the CuNb KS interface.

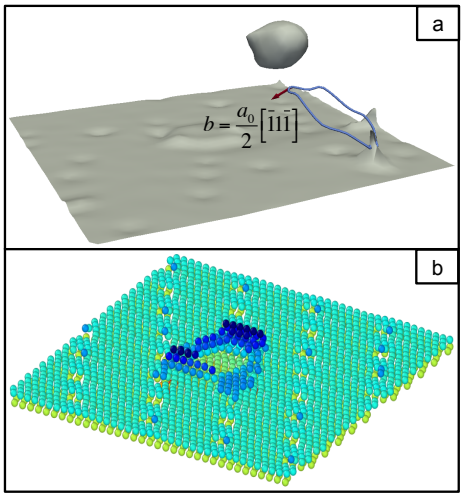

FIG. 17: (Color online) a) DXA analysis of the prismatic loop generated at a void in the Nb layer; and b) Crater structure formed in the Cu side of the interface upon absorption of the prismatic loop with the atoms colors according to their position perpendicular to the interface.

V. CONCLUSIONS

In summary, we report in this paper on the mechanical response of a bilayer CuNb nanocomposite to external compressive strain. We have analyzed the different deformation pathways that the system follows in the presence of various distributions of vacancy clusters. We observed that the presence of heavy-ion irradiation-induced defects substantially modifies the stress-strain response of the system since those defects alter the nucleation of the plasticity carrier. We have seen that when the number of vacancy defects at the interface is large, the system nucleates an extrinsic stacking fault instead of the less energetic intrinsic stacking fault as in the case of the pristine sample (or when the atomic density at the interface is larger). SFTs might act as a dislocation nucleation source at a level of stress considerably lower than the one required to nucleate dislocations at the pristine interface. The SFT unfaulting mechanism depends on the resolved shear stress on the tetrahedron faces, which is a function of the sample orientation. In the case of a {001} orientation, the SFT becomes a dislocation source, while on a {111} orientation in a nanocomposite, two threading dislocations generate from the SFT that finally disappear. The presence of voids also reduces the dislocation nucleation stress. Prismatic dislocation loops might be created at voids before any dislocation is nucleated at the interface, which lowers the system yield stress.

These results lead to the conclusion that in a heavy-ion irradiation environment, the mechanical response of heterophase nanocomposites may be substantially modified with respect to light-ion irradiation conditions, softening the material as dislocations nucleate at irradiation-created defects. These irradiation-induced dislocations react with the interface in different manners. Dissociated dislocations generated at an SFT react with the misfit dislocations at the interface to lower the total amount of strain energy. A perfect segment also generated at the SFT is fully absorbed and induces the re-emission of a dislocation segment with different Burgers vector. Prismatic loops are also absorbed at the interface creating a crater-like structure with Cu atoms penetrating into the Nb layer. This crater structure seems to be stable and remain so for large strains until eventually lead to the nucleation of new dislocations from the Cu side of the interface. Therefore, heterophase interfaces help in material self-healing since they react and partially absorb the dislocations generated at defects upon application of external loading.

VI. ACKNOWLEDMENTS

The authors thank J. P. Hirth, M. J. Demkowicz and A. Misra for exciting discussions. The authors also gratefully acknowledge the support from the Center for Materials at Irradiation and Mechanical Extremes, an Energy Frontier Research Center funded by the U.S. Department of Energy (Award Number 2008LANL1026) at Los Alamos National Laboratory. Parallel computations were performed on the Lobo machine at the High Performance Computing clusters at Los Alamos National Laboratory.

* Electronic address: enriquem@lanl.gov

[1] G. S. Was, Fundamentals of Radiation Materials Science, Springer, 2007.
[2] A. Misra, M. J. Demkowicz, J. Wang, R. G. Hoagland, The mulstiscale modeling of plastic deformation in metallic nanolayered composites, JOM April (2008) 39–42.
[3] A. Misra, X. Zhang, M. J. Demkowicz, R. G. Hoagland, M. Nastasi, Design of nano-composites for ultra-high strengths and radiations tolerance, Mater. Res. Soc. Symp. Proc. 1188.
[4] M. Demkowicz, P. Bellon, B. Wirth, Atomic-scale design of radiation-tolerant nanocomposites, MRS Bulletin 35 (2010) 1–7.
[5] N. Li, M. Nastasi, A. Misra, Defect structures and hardening mechanisms in high dose helium ion implanted cu and cu/nb multilayer thin films, Inter. J. Plast. 32-33 (2012) 1–16.
[6] W. Z. Han, M. J. Demkowicz, N. A. Mara, E. G. Fu, S. Sinha, A. D. Rollet, Y. Q. Wang, J. S. Carpenter, I. J. Beyerlein, A. Misra, Design of radiation tolerant materials via interface engineering, Adv. Mat. 25 (2013) 6975–6979.
[7] L. Zhang, M. J. Demkowicz, Morphological stability of cu-nb nanocomposites under high-energy collision cascades, Appl. Phys. Lett. 103 (2013) 061604.
[8] C. H. Woo, B. N. Singh, Production bias due to clustering of point defects in irradiation-induced cascade, Phil. Mag. A 65 (4) (1992) 889–912.
[9] A. Iwase, S. Ishino, J. Nucl. Mater. 276 (2000) 178–185.
[10] R. E. Stoller, G. R. Odette, B. D. Wirth, J. Nucl. Mater. 251 (1997) 49–60.
[11] A. Souidi, M. Houb, C. S. Becquart, L. Malerba, C. Domaine, R. E. Stoller, J. Nucl. Mater. 419 (2011) 122–133.
[12] A. E. Sand, S. L. Dudarev, K. Nordlund, EPL 103 (2013) 46003.
[13] AA. E. Sand, S. L. Dudarev, K. Nordlund, J. Nucl. Mater. 455 (2014) 207–211.
[14] D. Frenkel, B. Smit, Understanding Molecular Simulation, Academic Press, 2001.
[15] A. F. Voter, Hyperdynamics: Accelerated molecular dynamics of infrequent events, Phys. Rev. Lett. 78 (20) (1997) 3908.
[16] A. F. Voter, Parallel replica method for dynamics of infrequent events, Phys. Rev. B 57 (22) (1998) R13985.
[17] A. F. Voter, F. Montalenti, T. C. Germann, Extending the time scale in atomistic simulations of materials, Annu. Rev. Mater. Res. 32 (2002) 321.
[18] G. Henkelman, H. Jonsson, Long time scale kinetic monte carlo simulations without lattice approximation and predefined event table, J. Chem. Phys. 115 (21) (2001) 9657.
[19] L. Vernon, S. D. Kenny, R. Smith, E. Sanville, Growth mechanisms for tio2 at its rutile (110) surface, Phys. Rev. B 83 (2011) 075412.
[20] F. El-Mellouhi, N. Mousseau, L. J. Lewis, Kinetic activation-relaxation technique: An off-lattice self-learning kinetic monte carlo algorithm, Phys. Rev. B 78 (2008) 153202.
[21] H. Xu, Y. N. Osetsky, R. E. Stoller, Simulating complex atomistic processes: On-the-fly kinetic monte carlo scheme with selective active volumes, Phys. Rev. B 84 (2011) 132103.
[22] S. Plimpton, Fast parallel algorithms for short-range molecular dynamics, Journal of Computational Physics 117 (1995) 1–19.
[23] L. Zhang, E. Martinez, A. Caro, X.-Y. Liu, M. J. Demkowicz, Liquid-phase thermodynamics and structures in the cu–nb binary system, Modelling Simul. Mater. Sci. Eng. 21 (2013) 025005.
[24] R. F. Zhang, J. Wang, I. J. Beyerlein, A. Misra, T. C. Germann, Atomic-scale study of nucleation of dislocations from fcc–bcc interfaces, Acta Mater. 60 (2012) 2855–2865.
[25] I. J. Beyerlein, J. Wang, R. F. Zhang, Interface-dependent nucleation in nanostructured layered composites, Appl. Phys. Let. Mat. 1 (2013) 032112.
[26] A. Stukowski, K. Albe, Extracting dislocations and non-dislocation crystal defects from atomistic simulation data, Modelling Simul. Mater. Sci. Eng. 18 (2010) 085001.
[27] A. Stukowski, Visualization and analysis of atomistic simulation data with ovito–the open visualization tool, Modelling Simul. Mater. Sci. Eng. 18 (2010) 015012.
[28] L. A. Zepeda-Ruiz, E. Martinez, M. Caro, E. G. Fu,

A. Caro, Deformation mechanisms of irradiated metallic nanofoams, Appl. Phys. Lett. 103 (2013) 031909.

[29] A. Caro, J. Hetherly, A. Stukowski, M. Caro, E. Martinez, S. Srivilliputhur, L. Zepeda-Ruiz, M. Nastasi, Properties of helium bubbles in fe and fecr alloys, J. Nucl. Mater. 418 (2011) 261–268.

[30] E. Martinez, J. Marian, A. Arsenlis, M. Victoria, J. M. Perlado, A dislocation dynamics study of the strength of stacking fault tetrahedra. part i: interactions with screw dislocations, Phil. Mag. 88 (2008) 809–840.

[31] E. Martinez, J. Marian, J. M. Perlado, A dislocation dynamics study of the strength of stacking fault tetrahedra. part ii: interactions with mixed and edge dislocations, Phil. Mag. 88 (2008) 841–863.

[32] R. E. Voskoboinikov, Y. N. Osetsky, D. J. Bacon, Computer simulation of primary damage creation in displacement cascades in copper. i. defect creation and cluster statistics, J. Nucl. Mater. 377 (2008) 385–395.

[33] X.-M. Bai, A. F. Voter, R. G. Hoagland, M. Nastasi, B. P. Uberuaga, Efficient annealing of radiation damage near grain boundaries via interstitial emission, Science 327 (2010) 1631.